

QBO-dependent relation between electron precipitation and wintertime surface temperature

V. Maliniemi,¹ T. Asikainen,¹ K. Mursula,¹ and A. Seppälä²

Received 14 September 2012; revised 26 April 2013; accepted 22 May 2013; published 26 June 2013.

[1] Recent research has shown that energetic particle precipitation into the upper atmosphere can change ion and neutral chemistry, e.g., by enhancing NO_x concentration in the mesosphere, which, in turn, can affect stratospheric ozone balance under appropriate conditions. It has been suggested that this may affect the surface temperatures at high latitudes by modulating tropospheric circulation. Motivated by such results, we compare here the wintertime energetic electron precipitation (EEP) with North Atlantic Oscillation (NAO) and surface air temperature (SAT) in the Northern Hemisphere. We use the recently recalibrated energetic electron data from the Medium Energy Proton and Electron Detector instrument of the National Oceanic and Atmospheric Administration (NOAA)/Polar Orbiting Environment Satellites in two energy ranges (30–100 keV and 100–300 keV), the NAO index from NOAA, and the NASA Goddard Institute for Space Studies surface temperature analysis for years 1980–2010. We find a statistically significant correlation between EEP and the NAO index and also between EEP and SAT in certain geographic regions. The strongest negative correlation is found in Northeast Canada/Greenland, while the strongest positive correlation is found in North Siberia/Barents Sea, in agreement with similar studies using global geomagnetic activity as a proxy for particle precipitation. We find higher correlation when the two winters (1984/1985 and 2003/2004) of unprecedentedly strong sudden stratospheric warmings are excluded. We also find that the different phases of quasi-biennial oscillation (QBO; observed at 30 hPa) lead to dramatically different correlation patterns, with easterly QBO producing considerably stronger and spatially wider correlation and larger temperature response than westerly QBO.

Citation: Maliniemi, V., T. Asikainen, K. Mursula, and A. Seppälä (2013), QBO-dependent relation between electron precipitation and wintertime surface temperature, *J. Geophys. Res. Atmos.*, 118, 6302–6310, doi:10.1002/jgrd.50518.

1. Introduction

[2] The coupling of the near-Earth space environment and the atmosphere is of major scientific interest. Several recent studies have suggested links between the solar and external forcing and climate variability via several mechanisms (for reference, see, e.g., Gray *et al.* [2010]). In addition to the total solar irradiance variability, other mechanisms include, e.g., solar UV changes causing ozone changes in the stratosphere and affecting circulation in the troposphere [Matthes *et al.*, 2004, 2006], galactic cosmic rays affecting low cloud formation [Marsh and Svensmark, 2000], and solar wind affecting the global electric circuit [Tinsley, 2000]. While

these mechanisms can possibly affect tropospheric conditions on a global scale, more pronounced effects are found in regional-scale variability, especially in the Northern Hemisphere during winter.

[3] Several studies have indicated that solar activity can affect tropospheric winter conditions in the Northern Hemisphere. For example, van Loon and Labitzke [1988] showed that sea level pressure and surface temperature in certain North American stations in January and February correlated strongly with the 10.7 cm solar radio flux when the data were grouped according to the QBO (quasi-biennial oscillation) phase. Kodera [2002] and Huth *et al.* [2006] showed that during winter, the solar activity affects the strength of the North Atlantic Oscillation (NAO), which is considered to be the main mode of low-frequency circulation variability in the Northern Hemisphere winter [Barnston and Livezey, 1987]. Similar effects on the NAO have also been observed due to the variability of solar wind and geomagnetic activity [Boberg and Lundstedt, 2003; Thejll *et al.*, 2003]. NAO has been known to greatly affect the winter temperatures in North Europe and North Siberia as well as eastern North America and Greenland [see, e.g., Hurrell *et al.*, 2003]. (To highlight the strong effect the NAO has on winter

¹Department of Physics, Centre of Excellence in Research, University of Oulu, Oulu, Finland.

²Earth Observation, Finnish Meteorological Institute, Helsinki, Finland.

Corresponding author: V. Maliniemi, Department of Physics, Centre of Excellence in Research, University of Oulu, PO Box 3000, FI-90014 Oulu, Finland. (ville.maliniemi@oulu.fi)

surface air temperature (SAT) in the Northern Hemisphere, we reproduce the SAT anomalies caused by NAO variations later in this paper.) *Bochnicek et al.* [1999], *Seppälä et al.* [2009], and *Baumgaertner et al.* [2011] also showed that geomagnetic activity can affect the tropospheric winter temperatures, the anomalies of which resembled those caused by NAO variability. Geomagnetic activity indices *Ap/Kp* in these studies were used as a proxy for particle precipitation.

[4] Energetic particle precipitation into the atmosphere has been observed to cause significant changes in atmospheric chemistry, e.g., by leading to a significant enhancement of nitrogen oxides (NO_x) in the upper atmosphere [*Seppälä et al.*, 2007]. NO_x , in turn, can descend down and affect the ozone balance in the stratosphere during polar winter, when NO_x lifetimes are long due to absence of sunlight and the large-scale atmospheric motions are downward in the polar regions [*Randall et al.*, 2005]. *Rozanov et al.* [2005] used a chemistry-climate model to show that the increase in particle precipitation can cause notable changes in stratospheric ozone mixing ratios and temperatures as well as surface air temperatures by up to 2.5 K. A recent study by *Seppälä et al.* [2009] suggests that there is a statistically significant connection between global geomagnetic activity and polar surface air temperature variability in winter. They found a difference of up to 4.5 K in SAT between years of high and low geomagnetic *Ap* indices in some regions at polar latitudes. *Baumgaertner et al.* [2011] obtained similar results when using a chemistry-climate model. They also stated that the enhanced geomagnetic activity leads to polar stratospheric ozone loss which strengthens the polar vortex and the Northern Annular Mode (NAM), and these NAM anomalies can also be observed on the surface. *Calisto et al.* [2011] suggested also in their chemistry-climate model that cosmic rays modulate the NAM. NAM and NAO greatly resemble each other, although they are defined in a slightly different way [*Ambaum et al.*, 2001]. *Mironova et al.* [2012] recently found an association between energetic electron precipitation (EEP) and the vorticity of winter storms on the day-to-day timescale, which suggests a much faster mechanism than ozone destruction.

[5] During winter, the high-latitude stratosphere and troposphere are controlled by the polar vortex, which is also connected to the NAM [*Baldwin and Dunkerton*, 2001]. The polar vortex has an important role in transporting, e.g., NO_x enhancements to the lower atmosphere [*Randall et al.*, 2005] as well as keeping them at polar latitudes. Sudden stratospheric warmings (SSWs) can cause rapid changes in stratospheric and tropospheric dynamics [*Limpasuvan et al.*, 2004] and can greatly disturb the general circulation in the stratosphere during winter. During SSW, the high-latitude stratospheric western mean zonal wind weakens and even turns to easterly in some cases. This slows down the polar vortex [*Manney et al.*, 2005]. Weak vortex signals can also propagate down to the troposphere and turn the NAO/NAM more negative [*Baldwin and Dunkerton*, 2001]. *Holton and Tan* [1980] also found that the strength of the polar vortex and the frequency of SSWs are affected by the phase of the QBO, which is a dynamical circulation mode in the equatorial stratosphere. When studying particle precipitation effects, it is then important to also consider SSWs and the different phases of the QBO.

[6] This paper continues the earlier work on the particle precipitation effects by studying whether there is an observable correlation between EEP and the NAO index and between EEP and SAT in the Northern Hemisphere winter by using actual precipitating electron measurements. Using POES (Polar Orbiting Environment Satellites) satellite data for particle precipitation has been difficult in the past due to several problems with the data. The energetic protons [*Asikainen and Mursula*, 2011; *Asikainen et al.*, 2012] and energetic electrons (T. Asikainen and K. Mursula, Correction of NOAA/MEPED energetic electron fluxes for detector efficiency and proton contamination, submitted to *Journal of Geophysical Research*, 2013) of the MEPED (Medium Energy Proton and Electron Detector) instrument have recently been corrected for detector degradation and other problems and now form the longest running time series of over 30 years of energetic particle observations and will be utilized in this paper. The effect of SSWs and the QBO phase are also studied. The paper is organized as follows. The MEPED and other data used here are presented in section 2. In section 3, we discuss the long-term variation of EEP, and in section 4, we study the relation between NAO and EEP and the relation between surface temperatures and EEP as well as compare it with the effect of NAO on SAT. In section 5, we study the dependence of the EEP effect on SAT during the two QBO phases. Conclusions are given in section 6.

2. Data Description

[7] We used here the measurements of energetic electrons made by the NOAA/POES (National Oceanic and Atmospheric Administration/Polar Orbiting Environment Satellites) which have been operating since 1979. The POES fly in Sun-synchronous polar orbits at an altitude of about 850 km. In this study we used the NOAA-06, NOAA-08, NOAA-10, NOAA-12, and NOAA-15 satellites, which all fly in the dawn-dusk (07–19 LT) local time plane. The satellites carry the MEPED instrument [*Raben et al.*, 1995; *Evans and Greer*, 2000] which measures electrons in three integral energy channels corresponding to energy ranges of >30 keV (I1), >100 keV (I2), and >300 keV (I3), respectively. By subtracting the I2 flux from the I1 flux and the I3 flux from the I2 flux, we obtained the (differential) electron fluxes in the energy ranges of 30–100 keV (D1) and 100–300 keV (D2). It has been estimated that electrons in the D1 range penetrate down to 75–90 km altitude and in the D2 range to 65–75 km, i.e., to the upper and middle mesosphere, respectively [*Turunen et al.*, 2009].

[8] MEPED measures electrons in two nearly orthogonal directions. We used here only the local vertical detector (0°), which points roughly radially away from the Earth and measures mainly precipitating electrons at high latitudes where most precipitation is concentrated to. We excluded the measurements below 40° northern latitude, thus excluding, e.g., the South Atlantic anomaly region, where the particle fluxes are strong due to the weak magnetic field. We note that the electron detector is sensitive to protons of certain energy range. It is possible to remove proton contamination from the electron measurements if correct proton fluxes are known. Measured uncalibrated proton fluxes tend to be significantly underestimated due to MEPED proton

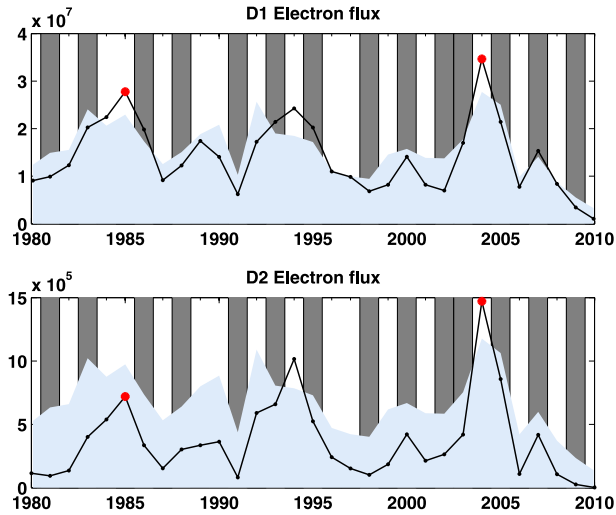


Figure 1. Averaged relative energetic electron fluxes during the three winter months in the (top) D1 and (bottom) D2 energy channels. Scaled A_p indices are indicated with light blue shading. The grey bars represent winters with the average QBO index (observed at 30 hPa) being westerly and other winters being easterly. The red circles represent the exceptional winters of 1985 and 2004.

detector degradation. Recently, the entire NOAA/MEPED proton database was consistently corrected and recalibrated [Asikainen and Mursula, 2011; Asikainen et al., 2012]. We used these recalibrated fluxes to remove the proton contamination from electron measurements. In the older satellites (here up to NOAA-12), the I1 channel is contaminated by protons between 135 and 1850 keV, the I2 channel by protons between 225 and 1850 keV, and the I3 channel by protons between 430 and 1850 keV. In the satellites from NOAA-15 onward, the contaminating energy ranges are 210–2700 keV, 280–2700 keV, and 440–2700 keV, respectively. After computing the recalibrated proton fluxes at these energy ranges, they were subtracted from the count rates of the respective electron channels. In addition to the proton contamination, the electron fluxes in the old and the new (here only NOAA-15) satellites also differ due to the differences in instrument efficiency caused by slightly different instrument construction. We have recently calculated instrument response for the electron channels of the old and new MEPED instruments. Detailed discussion of the correction of electron fluxes is presented by Asikainen and Mursula (submitted manuscript, 2013).

[9] For the NAO index and the QBO index, we used the NOAA Climate Prediction Center data (<http://www.cpc.ncep.noaa.gov/products/precip/CWlink/pna/nao.shtml> and <http://www.cpc.ncep.noaa.gov/data/indices/qbo.u30.index>). The NAO index has been calculated as the leading component of a rotated principal component analysis of 500 hPa height anomalies in the Northern Hemisphere (20°N – 90°N), representing middle tropospheric conditions [e.g., Barnston and Livezey, 1987]. Correlation between NAO and slightly differently defined NAM (also called Arctic oscillation) is high despite the fact that the loading patterns corresponding to the indices are somewhat different [e.g., Ambaum et al., 2001]. The QBO index has been measured

as the zonally averaged wind speed at 30 hPa above the equator. We used monthly values of both indices to calculate the 3 month average values used here.

[10] For the temperature, we used the NASA Goddard Institute for Space Studies surface air temperature analysis data (<http://data.giss.nasa.gov/gistemp/>) provided as gridded monthly temperature maps in $5^{\circ} \times 5^{\circ}$ boxes of geographical latitude and longitude. The temperature anomalies have been calculated from the local mean temperature during the reference period of 1961–1990. They are constructed from ground station data of the Global Historical Climatology Network, from Hadley Center analysis of global sea-ice coverage and sea surface temperatures (HadISST1) for 1880–1981, and from satellite measurements of sea surface temperature from 1982 onward (Optimum Interpolation Sea Surface Temperature Version 2). The temperature maps use spatial smoothing with a radius of 1200 km so that the temperature anomaly at a given location is computed as a weighted average of anomalies of all stations located within 1200 km of that point, with the weight decreasing linearly as a function of distance from 1 to 0 at 1200 km distance [Hansen et al., 2001, 2010].

3. Overview of Energetic Electron Precipitation

[11] We computed the average fluxes of precipitating D1 and D2 electrons during the three winter months (November, December, and January) in each year for 1980–2010 within $5^{\circ} \times 5^{\circ}$ latitude-longitude grid boxes poleward of 40° northern latitude. (The year of each winter was deter-

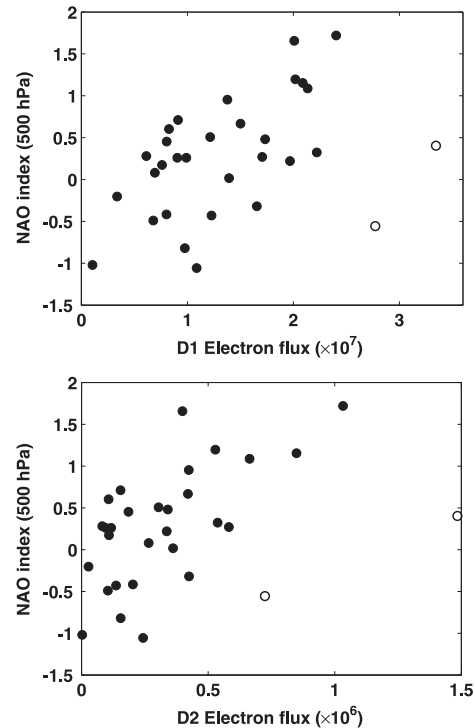


Figure 2. Scatterplots of the NAO index as a function of EEP fluxes in the (top) D1 energy range and (bottom) D2 energy range. The open circles represent the winters of 1985 and 2004.

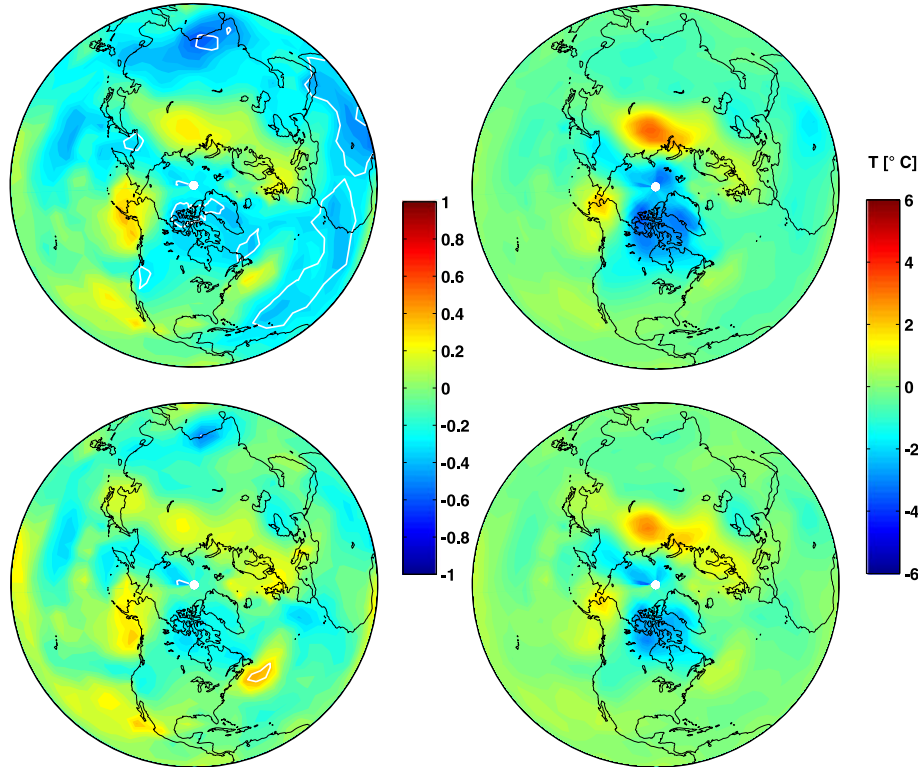


Figure 3. (left) Correlation coefficients between the EEP fluxes and SAT for the (top) D1 and (bottom) D2 channels. The white lines represent the 95% confidence levels. (right) Range of SAT variation related to EEP flux variation in the (top) D1 and (bottom) D2 channels.

mined by January so that, e.g., winter of 1990 was an average over November–December 1989 and January 1990.) We defined the EEP region to consist of grid boxes where the average flux was larger than the background level of 2000 cts/(cm² sr s) for D1 and 800 cts/(cm² sr s) for D2. (Note that this region forms an oval describing the geographic distribution of precipitation in the narrow LT range of the NOAA/POES spacecraft and does not represent the momentary LT distribution of EEP.) We then multiplied the flux values of these grid boxes by $\cos(\lambda)$ (λ is the geographic latitude of the equatorward edge of the grid box) in order to take into account the grid box area on the spherical surface and summed them to 3 monthly winter fluxes for each year. (Accordingly, the total EEP fluxes are relative rather than absolute fluxes.)

[12] The time series of the total EEP fluxes for both energy ranges are shown in Figure 1 along with the corresponding 3 month average A_p indices. The A_p indices have been scaled properly (unitless) to compare overall evolution between A_p and EEP fluxes. One can see that the two EEP time series are quite similar, although the relative heights of the cycle peaks are somewhat different. The electron fluxes show a clear solar cycle variation with the maximum fluxes observed in the declining phases of the solar cycle in 1985, 1994, and 2004. The largest wintertime fluxes over the entire 31 year period were observed in 2004, due to the major magnetic storm on 20 November 2003 having a minimum Dst index of about -420 nT. On the other hand, the two other maxima in 1985 and 1994 were associated with intense

recurrent high-speed solar wind streams. One can see from Figure 1 that while the temporal evolution of the electron fluxes in both energy ranges has considerable similarity with the A_p index, clear differences between the fluxes and the A_p index exist. The cycle maxima of the fluxes and A_p are found in the declining phases of the solar cycle but can deviate by up to 2 years (maximum A_p in 1983 and maximum electron flux in 1985; maximum A_p in 1992 and maximum electron flux in 1994). The D2 flux correlates visibly less with the A_p index than the D1 flux, which is understandable since the A_p index measures mainly the intensity of electric currents in the ionosphere produced by auroral particles, which have slightly less energy than D1 electrons. We note that the A_p index, which has previously been used as a proxy of all energetic particle precipitation in atmospheric studies, is actually a rather crude proxy for the electron fluxes at these energies.

4. Comparing NAO and Temperature With Electron Precipitation

[13] We first compared the NAO index with EEP by computing the correlation coefficient between the 3 month averaged (November–December–January (NDJ)) NAO index and EEP. We then used bootstrapping with 1000 resamplings of variables to get the correct p-values of correlation. Resampling was done by shuffling the harmonic phases of the two time series. The time series resampled this way have certain similarities with original series (e.g., autocorrelation and variance) while being physically unrelated with it [see,

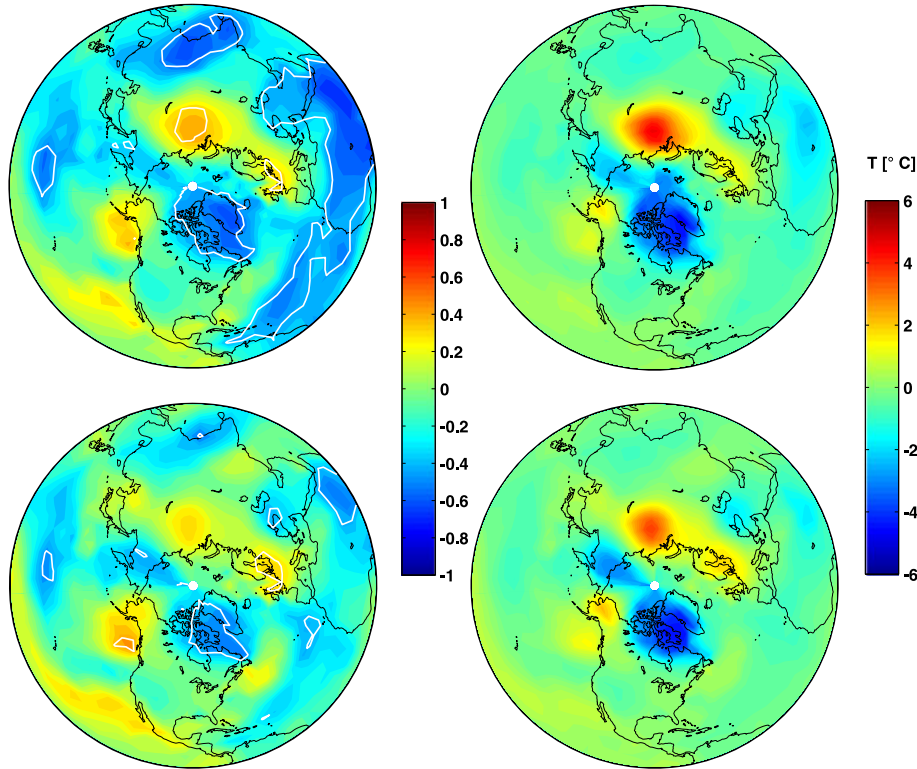


Figure 4. Same as Figure 3 but excluding the winters of 1985 and 2004.

e.g., Thejll *et al.*, 2003]. The p-values were obtained by calculating the proportion of correlation coefficients in the resamplings that were larger than the observed original correlation coefficient. The top (bottom) plot in Figure 2 shows the NAO indices as a function of D1 (D2) fluxes. Both plots depict a fairly strong correlation ($cc = 0.44$ and $p = 0.015$ for D1 and $cc = 0.44$ and $p = 0.031$ for D2). We also wanted to study whether strong SSW events have observable effect on this correlation. Manney *et al.* [2005] showed that winters of 1984/1985, 1986/1987, and 2003/2004 experienced the strongest SSW events since 1979 (until 2004). They also showed that in January 1985 and 2004, the mean zonal wind at high latitudes in the stratosphere was easterly (only two winters in their time series), which indicates prolonged

vortex disruption, while the SSW in 1987 shows easterlies only in February. We applied a similar zonal wind analysis between 60°N and 90°N latitudes at 50 hPa, by using the same data (National Centers for Environmental Prediction/National Center for Atmospheric Research reanalysis) for years 1980–2010. The same two years (1984/1985 and 2003/2004) were still the only ones with easterly mean zonal wind in January. Also, these years were the only ones where the value differs from the mean January zonal wind value during 1980–2010 by more than two standard deviations. By excluding these two exceptional winters, we got a stronger correlation ($cc = 0.64$ and $p < 0.001$ for D1 and $cc = 0.65$ and $p < 0.001$ for D2) (see also Figure 2).

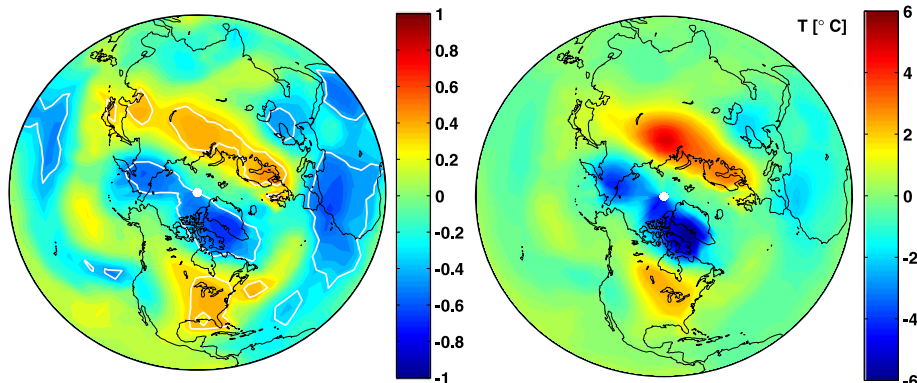


Figure 5. (left) Correlation coefficients between the wintertime NAO index and SAT. The white lines represent the 95% confidence levels. (right) Range of SAT variation related to NAO index variation.

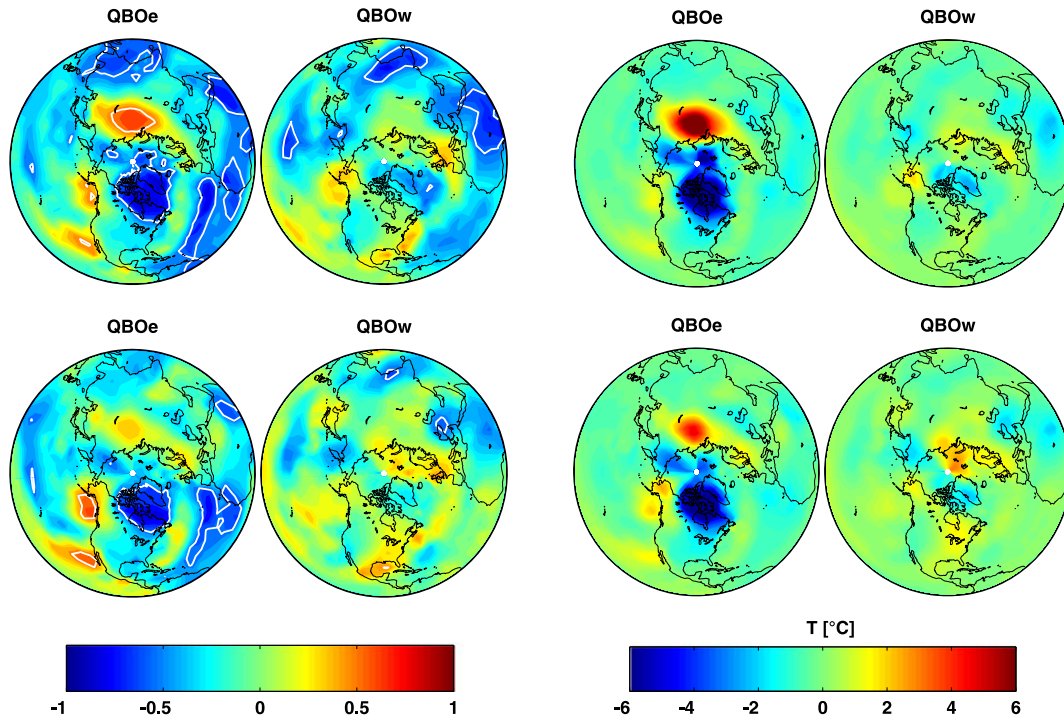


Figure 6. Same as Figure 4 but dividing winters into easterly and westerly QBO phase times.

[14] In order to study the effect of the EEP on SAT, we computed the correlation coefficient between the EEP and the 3 month averaged temperature (NDJ) in each $5^\circ \times 5^\circ$ geographical grid box. The best fit line and the correlation coefficient between EEP and SAT were determined for each grid box. The p-values were computed in the same way for each grid box as was done with NAO and EEP. The left-hand side of Figure 3 (top for D1 and bottom for D2) shows the geographic distribution of the correlation coefficient between the winter EEP and the winter temperature anomalies. The right-hand side shows the corresponding range of temperature variation attributed to the correlation with EEP. Negative values in the range represent anticorrelation between EEP and SAT. The temperature range ΔSAT was calculated by multiplying the slope of the fit by the total range of the EEP (ΔEEP) during 1980–2010 ($k = \frac{\Delta\text{SAT}}{\Delta\text{EEP}}$, where k is the slope). The white lines in the correlation coefficient maps represent the 95% confidence levels. In Figure 3, all winters are included in the analysis. One can see two regions of moderate correlation in D1: negative correlation in Greenland/Northeast Canada and positive correlation in North Siberia (also visible in D2). Also, the large area of negative correlation at lower latitudes from the Atlantic to the Middle East and the small area of positive correlation in Alaska (also visible in D2) are visible in D1. However, most of the regions in Figure 3 are not significant in the 95% confidence level, especially in the D2 energy range.

[15] *Seppälä et al.* [2009] used a 2 month lag between A_p (October–November–December–January) and surface temperature (December–January–February (DJF)) and found that the temperature differences between years of high and low A_p indices were larger when SSW years were excluded. We neglected the years with the strongest SSW events (1985 and

2004; see above). Figure 4 shows the same analysis as in Figure 3 after the winters of 1985 and 2004 were excluded. The correlations are now much stronger and more significant, and the regions are more extended than those in Figure 3. One can see several regions of strong (and significant) correlation. Large regions of strong positive correlation are found in Northern Siberia, around the North Sea/Great Britain, and in Alaska, while regions of strong negative correlation are found in Greenland/Baffin Bay. There is also an extensive area of negative correlation at lower latitudes expanding from the Atlantic to the Middle East. The maximum ranges of variation in the SAT in Figure 4 for D1 are $4.5 \pm 2.3^\circ\text{C}$ in Baffin Bay with -0.55 ($p = 0.014$) correlation and $4.3 \pm 2.9^\circ\text{C}$ in North Siberia with 0.44 ($p = 0.045$) correlation. For D2, the corresponding ranges are $4.1 \pm 2.2^\circ\text{C}$ with -0.52 ($p = 0.011$) correlation in Baffin Island and $3.8 \pm 3.4^\circ\text{C}$ with 0.32 ($p = 0.114$) correlation in North Siberia. The 95% confidence intervals for the range values were calculated in the same way as described above for the p-values by bootstrapping the residuals of the original fit and then fitting with the new series consisting of the original fit parameters and the shuffled residuals. The slope value, which corresponded to the value of 0.975 in the cumulative distribution of resampled slopes, determined the confidence interval. The overall pattern depicted in Figure 4 also resembles the one observed between SAT and global geomagnetic activity [*Seppälä et al.*, 2009; *Baumgaertner et al.*, 2011].

[16] The pattern in Figure 4 now resembles the winter temperature pattern caused by NAO variations observed before in several studies [see, e.g., *Hurrell*, 1995; *Hurrell et al.*, 2003; *Wang et al.*, 2005; *Wettstein and Mearns*, 2002]. We reproduced this relation by using the same method as in Figures 3 and 4 to better visualize it and compare it with the results obtained between SAT and EEP. The correlation and

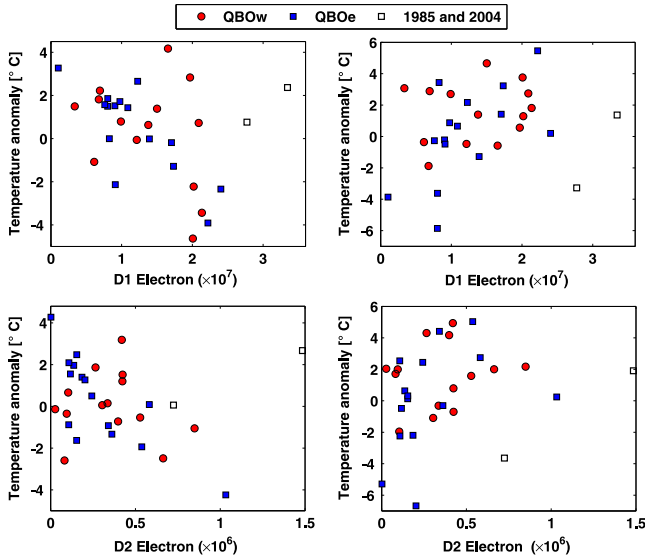


Figure 7. Scatterplots between SAT and the EEP fluxes in the grid boxes of largest range of SAT variation in Figure 4. (left) Negative correlation in Baffin Bay (67.5°N latitude, 47.5°W longitude) and Baffin Island (57.5°N latitude, 62.5°W longitude) for D1 and D2, respectively. (right) Positive correlation in North Siberia (67.5°N latitude, 87.5°E longitude and 62.5°N latitude, 92.5°E longitude) for D1 and D2, respectively. The open squares represent the winters of 1985 and 2004. The blue squares represent winters with easterly QBO and the red circles winters with westerly QBO.

SAT range maps for the NAO effect on SAT are presented in Figure 5 (all years included). One can see roughly the same regions of strong correlation in Figure 5 as in Figure 4: Large regions of strong positive correlation are found in Northern Siberia, around the Baltic Sea, and in eastern North America, while regions of strong negative correlation are found in Greenland/Baffin Bay and at lower latitudes expanding from the Atlantic to the Middle East. Differences include the positive correlation area in Alaska in Figure 4 (not visible in Figure 5) and the positive correlation area in eastern North America and the negative correlation area in Northeast Siberia in Figure 5 (not visible in Figure 4). This temperature pattern in Figure 5 is also consistent with those observed earlier by Hurrell [1995] and Hurrell *et al.* [2003], although they used different months in their averages (December-January-February-March). The maximum ranges of SAT variation related to the correlation with the NAO index are $4.9 \pm 4.0^{\circ}\text{C}$ with a positive slope ($cc = 0.45$ and $p = 0.012$) in Northern Siberia and $5.9 \pm 2.5^{\circ}\text{C}$ with a negative slope ($cc = -0.65$ and $p < 0.001$) between Greenland and Baffin Island, which are slightly larger than those in Figure 4 for D1.

[17] When we applied a similar correlation analysis for the 3 month average Ap index and SAT (excluding the winters of 1985 and 2004), the correlation pattern and the maximum range of variation in the SAT were fairly similar (although correlations were somewhat smaller) to those for the D1 electron flux in Figure 4: $4.6 \pm 3.8^{\circ}\text{C}$ for positive correlation in North Siberia ($cc = 0.40$ and $p = 0.059$) and

$4.2 \pm 3.1^{\circ}\text{C}$ for negative correlation in Baffin Island ($cc = -0.46$ and $p = 0.027$). The temperature ranges related to Ap that we found were in agreement with those observed earlier [Seppälä *et al.*, 2009] even using a somewhat different method and data set.

[18] We also studied how our results vary with different time lags between EEP and SAT by calculating different sets of 3 month averages for both EEP and SAT. We calculated the total correlation poleward from 50°N latitude by summing squares of all correlation coefficients significant at the 95% confidence level. Before summing, the correlation coefficients were weighted by a factor of $\cos(\lambda)$ in order to normalize the spatial size of the correlation pattern (see above). Taking into account both D1 and D2 and the spatial extension of the correlation patterns, the overall best total correlation (10.6 in 163 grid boxes for D1 and 4.6 in 62 grid boxes for D2) was found for the 0 month lag (NDJ-NDJ). The total correlation was also strong for the 1 month lag (NDJ-DJF: 11.5 in 124 grid boxes for D1 and 3.3 in 24 grid boxes for D2) and also for another 0 month lag (DJF-DJF: 9.1 in 74 grid boxes for D1 and 4.3 in 35 grid boxes for D2), but two other alternatives gave notably smaller total correlations (October-November-December (OND)-DJF: 7.8 in 75 grid boxes for D1 and 2.3 in 24 grid boxes for D2; OND-NDJ: 4.8 in 94 grid boxes for D1 and 0.1 in 1 grid box for D2). Note also that the correlation between the NAO and EEP was strongest for the 0 month lag (NDJ-NDJ).

5. QBO Phase Separation

[19] Figure 6 shows the maps of the correlation coefficient between EEP and SAT and the range of variation in SAT for the two phases of the QBO. The QBO phase was defined from the equatorial 3 month (NDJ) average wind at 30 hPa. (Winters of westerly and easterly QBOs are indicated in Figure 1.) The winters of 1985 and 2004 were excluded from the analysis. Figure 6 shows quite a similar high-latitude correlation pattern for the easterly QBO phase (for both D1 and D2) as in Figure 4. The large negative correlation area in Northeast Canada in Figure 4 strengthens for easterly QBO but becomes an insignificant area for westerly QBO. The positive correlation area in Northern Siberia in Figure 4 strengthens and expands east and west for the easterly QBO phase but disappears almost completely for westerly QBO. Also, the regions of positive correlation in Alaska and negative correlation in Northeast Siberia in Figure 4 are significantly weaker for westerly QBO. Note also that the two QBO phases depict quite a different correlation pattern even at lower latitudes. The large region of negative correlation from the Atlantic to the Middle East weakens for westerly QBO (and disappears in D2). Similar differences were also found in the correlation patterns between the two QBO phases if we used the Ap index instead of EEP. We applied a similar test for the two QBO phases as for the different time lags, where we obtained for D1 a total correlation of 32.9 in 210 grid boxes in easterly QBO and 0.6 in 3 grid boxes in westerly QBO and for D2 a total correlation of 17.3 in 89 grid boxes in easterly QBO and 0 in westerly QBO.

[20] Figure 7 presents the scatterplots between SAT and the EEP fluxes in those grid boxes which have the largest range of SAT variation in Figure 4. The plots on the left cor-

respond to the location of maximum range of SAT variation attributed to D1 in Baffin Bay (67.5°N latitude, 47.5°W longitude) and D2 in Baffin Island (57.5°N latitude, 62.5°W longitude), and the plots on the right show the same for D1 (67.5°N latitude, 87.5°E longitude) and for D2 (62.5°N latitude, 92.5°E longitude) in North Siberia. The two winters of 1985 and 2004 are marked as open squares in Figure 7. Figure 7 also shows the winters with their QBO phases. Note that although these plots correspond to the grid boxes of largest correlation in Figure 4, they are also well inside the areas of significant correlation for the easterly QBO phase in Figure 6 (except North Siberia in D2, which is insignificant also in Figure 4). However, they are in regions of insignificant correlation for the westerly QBO phase, which underlines the similarity of the overall patterns in Figure 4 with the easterly QBO in Figure 6. Figure 7 confirms that both positive and negative correlations are stronger for easterly QBO. The negative correlations in Figure 7 for D1 are -0.78 ($p = 0.002$; $6.0 \pm 2.6^\circ\text{C}$ range) in easterly QBO and -0.36 ($p = 0.208$; $2.5 \pm 3.7^\circ\text{C}$) in westerly QBO. The positive correlations for D1 are 0.59 ($p = 0.027$; $6.7 \pm 4.7^\circ\text{C}$) in easterly QBO and 0.17 ($p = 0.540$; $0.9 \pm 2.7^\circ\text{C}$) in westerly QBO. Similarly, for D2, the correlation is significant only in the easterly QBO phase ($cc = -0.77$, $p < 0.001$, and $6.6 \pm 3.2^\circ\text{C}$) in Baffin Bay. The easterly QBO phase for D2 in North Siberia gives 0.38 ($p = 0.169$; $4.8 \pm 5.7^\circ\text{C}$) correlation.

[21] The results in Figures 6 and 7 show that the QBO phase has an important effect on how the EEP correlates with surface temperatures. The easterly QBO phase strengthens the correlation pattern observed in the overall pattern in Figure 4, while during westerly QBO, the patterns change and weaken significantly and even disappear in some cases. It is known that the polar vortex strength depends on the QBO phase [Holton and Tan, 1980]. Stronger correlation seen between EEP and SAT in easterly QBO suggests that the effect of EEP on the surface temperatures also depends on the strength of the polar vortex.

6. Conclusions

[22] Using the recalibrated energetic electron fluxes from the NOAA/POES satellites for 1980–2010, we have shown here that electron precipitation shows significant correlation with the NAO index and the surface air temperature. Positive correlation was found in Northern Siberia/Barents Sea and Alaska and negative correlation in Northeast Canada/Greenland. Other large regions of high correlation but smaller associated temperature variation were found at lower latitudes. The observed correlations were more significant if the two years of the strongest SSW events (winters of 1985 and 2004) were excluded. The temperature response related to the EEP variation was more than 4°C increase in Northern Siberia and 4°C decrease in Northeast Canada/Greenland. Electrons with 30–100 keV and 100–300 keV energies had approximately the same correlation pattern with temperature, but the strength and areas of correlation were somewhat larger for lower energies. Also, the strong correlation obtained between the EEP and the NAO index and the overall similarity of the pattern observed between the EEP and SAT with the pattern observed between the NAO and SAT on winter tempera-

tures support a mechanism where SAT variation is caused by modulation of NAM/NAO by EEP. These results are consistent with earlier studies, which found a connection between global geomagnetic activity (used as a proxy for energetic particle precipitation) and surface air temperature [Seppälä et al., 2009; Baumgaertner et al., 2011]. However, other studies have indicated tropospheric variability (especially NAO) related to sunspot variability. Accordingly, the details of the stratospheric-tropospheric connection are still not fully known, and there is a need for additional research on this field.

[23] Most importantly, we showed here that the correlations and related temperature variations are considerably stronger during the easterly QBO phase than during the westerly QBO phase (observed at 30 hPa). The temperature response related to EEP in the easterly QBO phase is more than 6.5°C increase in Northern Siberia and about 6°C decrease in Northeast Canada/Greenland. Also, the global correlation patterns change significantly with the QBO phase. These results suggest that global preconditioning of the high-latitude atmosphere by the QBO phase is critically important for connecting the EEP variation to SAT variation.

[24] **Acknowledgments.** We thank NOAA NGDC for the MEPED data, NOAA CPC for the NAO and QBO data, and NASA GISS for the temperature data. We acknowledge the financial support by the Academy of Finland to projects 134547, 128189, 257403, and 264994; the Thule Institute of the University of Oulu; the ESPAS project by the European Commission; and COST Action ES1005.

References

- Ambaum, M. H. P., B. J. Hoskins, and D. B. Stephenson (2001), Arctic oscillation or North Atlantic oscillation?, *J. Clim.*, *14*, 3495–3507, doi:10.1175/1520-0442(2001)014<3495:AONAO>2.0.CO;2.
- Asikainen, T., and K. Mursula (2011), Recalibration of the long-term NOAA/MEPED energetic proton measurements, *J. Atmos. Sol. Terr. Phys.*, *73*, 335–347, doi:10.1016/j.jastp.2009.12.011.
- Asikainen, T., K. Mursula, and V. Maliniemi (2012), Correction of detector noise and recalibration of NOAA/MEPED energetic proton fluxes, *J. Geophys. Res.*, *117*, A09204, doi:10.1029/2012JA017593.
- Baldwin, M. P., and T. J. Dunkerton (2001), Stratospheric harbingers of anomalous weather regimes, *Science*, *294*, 581–584, doi:10.1126/science.1063315.
- Barnston, A. G., and R. E. Livezey (1987), Classification, seasonality and persistence of low-frequency atmospheric circulation patterns, *Mon. Weather Rev.*, *115*, 1083–1126, doi:10.1175/1520-0493(1987)115<1083:CSAPOL>2.0.CO;2.
- Baumgaertner, A. J. G., A. Seppälä, P. Jöckel, and M. A. Clilverd (2011), Geomagnetic activity related NO_x enhancements and polar surface air temperature variability in a chemistry climate model: Modulation of the NAM index, *Atmos. Chem. Phys.*, *11*, 4521–4531, doi:10.5194/acp-11-4521-2011.
- Boberg, F., and H. Lundstedt (2003), Solar wind electric field modulation of the NAO: A correlation analysis in the lower atmosphere, *Geophys. Res. Lett.*, *30*(15), 1825, doi:10.1029/2003GL017360.
- Bochnicek, J., P. Hejda, V. Bucha, and J. Pýcha (1999), Possible geomagnetic activity effects on weather, *Ann. Geophys.*, *17*, 925–932, doi:10.1007/s00585-999-0925-4.
- Calisto, M., I. Usoskin, E. Rozanov, and T. Peter (2011), Influence of galactic cosmic rays on atmospheric composition and dynamics, *Atmos. Chem. Phys.*, *11*, 4547–4556, doi:10.5194/acp-11-4547-2011.
- Evans, D., and M. Greer (2000), Polar orbiting environmental satellite space environment monitor—2: Instrument descriptions and archive data documentation, *Tech. Memo.*, OAR 456-SEC42, NOAA, Boulder, Colo.
- Gray, L. J., et al. (2010), Solar influences on climate, *Rev. Geophys.*, *48*, RG4001, doi:10.1029/2009RG000282.
- Hansen, J., R. Ruedy, M. Sato, M. Imhoff, W. Lawrence, D. Easterling, T. Peterson, and T. Karl (2001), A closer look at United States and global surface temperature change, *J. Geophys. Res.*, *106*, 23,947–23,964, doi:10.1029/2001JD000354.

- Hansen, J., R. Ruedy, M. Sato, and K. Lo (2010), Global surface temperature change, *Rev. Geophys.*, *48*, RG4004, doi:10.1029/2010RG000345.
- Holton, J. R., and H.-C. Tan (1980), The influence of the equatorial quasi-biennial oscillation on the global circulation at 50 mb, *J. Atmos. Sci.*, *37*, 2200–2208, doi:10.1175/1520-0469(1980)037<2200:TIOEQ>2.0.CO;2.
- Hurrell, J. W. (1995), Decadal trends in the North Atlantic Oscillation: Regional temperatures and precipitation, *Science*, *269*, 676–679, doi:10.1126/science.269.5224.676.
- Hurrell, J. W., Y. Kushnir, G. Ottersen, and M. Visbeck (2003), *The North Atlantic Oscillation: Climate Significance and Environmental Impact*, *Geophys. Monogr. Ser.*, vol. 134, AGU, Washington D. C.
- Huth, R., L. Pokorná, J. Bochníček, and P. Hejda (2006), Solar cycle effects on modes of low-frequency circulation variability, *J. Geophys. Res.*, *111*, D22107, doi:10.1029/2005JD006813.
- Kodera, K. (2002), Solar cycle modulation of the North Atlantic Oscillation: Implication in the spatial structure of the NAO, *Geophys. Res. Lett.*, *29*(8), 1218, doi:10.1029/2001GL014557.
- Limpasuvan, V., D. W. J. Thompson, and D. L. Hartmann (2004), The life cycle of the Northern Hemisphere sudden stratospheric warmings, *J. Clim.*, *17*, 2584–2597, doi:10.1175/1520-0442(2004)017<2584:TLCOTN>2.0.CO;2.
- Manney, G. L., K. Krüger, J. L. Sabutis, S. A. Sena, and S. Pawson (2005), The remarkable 2003–2004 winter and other recent warm winters in the Arctic stratosphere since the late 1990s, *J. Geophys. Res.*, *110*, D04107, doi:10.1029/2004JD005367.
- Marsh, N., and H. Svensmark (2000), Cosmic rays, clouds, and climate, *Space Sci. Rev.*, *94*, 215–230.
- Matthes, K., U. Langematz, L. L. Gray, K. Kodera, and K. Labitzke (2004), Improved 11-year solar signal in the Freie Universität Berlin climate middle atmosphere model (FUB-CMAM), *J. Geophys. Res.*, *109*, D06101, doi:10.1029/2003JD004012.
- Matthes, K., Y. Kuroda, K. Kodera, and U. Langematz (2006), Transfer of the solar signal from the stratosphere to the troposphere: Northern winter, *J. Geophys. Res.*, *111*, D06108, doi:10.1029/2005JD006283.
- Mironova, I., B. Tinsley, and L. Zhou (2012), The links between atmospheric vorticity, radiation belt electrons, and the solar wind, *Adv. Space Res.*, *50*, 783–790, doi:10.1016/j.asr.2011.03.043.
- Raben, V., D. Evans, H. Sahm, and M. Huynh (1995), TIROS/NOAA satellite space environment monitor data archive documentation, *Tech. Memo., ERL SEL-75*, NOAA, Boulder, Colo.
- Randall, C. E., et al. (2005), Stratospheric effects of energetic particle precipitation in 2003–2004, *Geophys. Res. Lett.*, *32*, L05802, doi:10.1029/2004GL022003.
- Rozanov, E., L. Callis, M. Schlesinger, F. Yang, N. Andronova, and V. Zubov (2005), Atmospheric response to NO_x source due to energetic electron precipitation, *Geophys. Res. Lett.*, *32*, L14811, doi:10.1029/2004GL023041.
- Seppälä, A., P. T. Verronen, M. A. Clilverd, C. E. Randall, J. Tamminen, V. Sofieva, L. Backman, and E. Kyrölä (2007), Arctic and Antarctic polar winter NO_x and energetic particle precipitation in 2002–2006, *Geophys. Res. Lett.*, *34*, L12810, doi:10.1029/2007GL029733.
- Seppälä, A., C. E. Randall, M. A. Clilverd, E. Rozanov, and C. J. Rodger (2009), Geomagnetic activity and polar surface air temperature variability, *J. Geophys. Res.*, *114*, A10312, doi:10.1029/2008JA014029.
- Thejll, P., B. Christiansen, and H. Gleisner (2003), On correlations between the North Atlantic Oscillation, geopotential heights, and geomagnetic activity, *Geophys. Res. Lett.*, *30*(6), 1347, doi:10.1029/2002GL016598.
- Tinsley, B. A. (2000), Influence of solar wind on the global electric circuit, and inferred effects on cloud microphysics, temperature, and dynamics in the troposphere, *Space Sci. Rev.*, *94*, 231–258.
- Turunen, E., P. T. Verronen, A. Seppälä, C. J. Rodger, M. A. Clilverd, J. Tamminen, C.-F. Enell, and T. Ulich (2009), Impact of different energies of precipitating particles on NO_x generation in the middle and upper atmosphere during geomagnetic storms, *J. Atmos. Sol. Terr. Phys.*, *71*, 1176–1189, doi:10.1016/j.jastp.2008.07.005.
- van Loon, H., and K. Labitzke (1988), Association between the 11-year solar cycle, the QBO, and the atmosphere. Part II: Surface and 700 mb in the Northern Hemisphere in winter, *J. Clim.*, *1*, 905–920, doi:10.1175/1520-0442(1988)001<0905:ABTYSC>2.0.CO;2.
- Wang, D., C. Wang, X. Yang, and J. Lu (2005), Winter Northern Hemisphere surface air temperature variability associated with the Arctic oscillation and North Atlantic Oscillation, *Geophys. Res. Lett.*, *32*, L16706, doi:10.1029/2005GL022952.
- Wettstein, J. J., and L. O. Mearns (2002), The influence of the North Atlantic-Arctic oscillation on mean, variance, and extremes of temperature in the Northeastern United States and Canada, *J. Clim.*, *15*, 3586–3600, doi:10.1175/1520-0442(2002)015<3586:TIOENA>2.0.CO;2.